Close binary black hole in a radio-quiet quasar: a candidate of Nano-Hertz gravitational wave emitter

Hai-Cheng Feng
Yunnan Observatories
Hong-Tao Liu
Yunnan Astronomical Observatory, Chinese Academy of Sciences
Jinming Bai (baijinming@ynao.ac.cn)
Yunnan Astronomical Observatory, Chinese Academy of Sciences

Physical Sciences - Article

Keywords: Close Supermassive Binary Black Holes, Radio-loud Quasars, Jet Model, Sinusoid-like Light Curve, Relativistic Orbital Speeds

Posted Date: February 12th, 2021

DOI: https://doi.org/10.21203/rs.3.rs-224548/v1

Close binary black hole in a radio-quiet quasar: a candidate of Nano-Hertz gravitational wave emitter

Hai-Cheng Feng[1,2,3,★], Hong-Tao Liu[1,3,4,★], Jin-Ming Bai[1,3,4,★]

[1] *Yunnan Observatories, Chinese Academy of Sciences, Kunming 650011, Yunnan, People's Republic of China*

[2] *University of Chinese Academy of Sciences, Beijing 100049, People's Republic of China*

[3] *Key Laboratory for the Structure and Evolution of Celestial Objects, Chinese Academy of Sciences, Kunming 650011, Yunnan, People's Republic of China*

[4] *Center for Astronomical Mega-Science, Chinese Academy of Sciences, 20A Datun Road, Chaoyang District, Beijing, 100012, People's Republic of China*

★ *e-mail: hcfeng@ynao.ac.cn; htliu@ynao.ac.cn; baijinming@ynao.ac.cn*

Close supermassive binary black holes (SMBBHs) with separations less than $\sim$ 0.1 parsec are expected to be Nano-Hertz gravitational wave sources[1]. SMBBH systems should exhibit periodic variability[2]. However, periodic variability in radio-loud quasars may be interpreted with the jet model[3]. Here we report the detection of a robust periodic signal in the optical variability of the radio-quiet quasar PG 0923+201 with an observed period of 726.8 $\pm$ 4.7 days, obtained from the sinusoid-like light curve of a temporal baseline of about 9 years. This periodicity is probably from a close SMBBH with a total mass of $10^{9.3}$ solar masses and a separation of $\sim$ 0.01 parsec, implying relativistic orbital speeds. Such a system has passed through the well-known "final parsec problem" of SMBBH systems[4], and the Nano-Hertz gravitational wave radiation becomes significant. The ratio of the separation between these two black holes to the broad-line region size is $\sim$ 0.1. A close SMBBH is also suggested by this small ratio and the spectral properties of Balmer broad lines in this quasar. This radio-quiet quasar is a candidate emitter of Nano-Hertz gravitational waves at a frequency of about 30 Nano-Hertz.

The existence of black hole had been confirmed by event-horizon-scale images of supermassive black hole (SMBH, with mass $\gtrsim 10^6 M_\odot$, $M_\odot$ is the solar mass) in the center of the elliptical

galaxy M87[5] and the first direct detection of gravitational waves of a binary black hole merger (with masses of about thirty to forty $M_{\odot}$)[6]. Searching for close supermassive binary black holes (SMBBHs) and observational identification are big challenges. The hydrodynamic and magneto-hydrodynamic simulations show that streams of gas are efficiently peeled by an SMBBH off the inner edge of a circumbinary disk, and rapidly traverse the central cavity in the circumbinary disk, forming individual mini disks surrounding each SMBH [7–12].

The SMBBH accretion from circumbinary disk can produce a more bursty and sawtooth pattern of the optical-ultraviolet light curves of active galactic nuclei and quasars[9,10,12,13]. The relativistic Doppler boosting due to the orbit motion of the secondary SMBH in a circular orbit can produce the sinusoidal light curves[2,14,15]. The first order approximation in $\beta = v/c$ of the relativistic Doppler boosting is equivalent to a sinusoid model that is favored by the sinusoid-like variability of the light curve of PG1302-102, and is strongly preferred over other models, such as the Doppler boosting model of SMBBH with non-zero eccentricity orbits, the accretion model of SMBBH, and the pure noise model[14].

Figure 1 shows the optical light curve of the Sloan Digital Sky Survey (SDSS)[16] radio-quiet quasar PG 0923+201 (=SDSS J092554.72+195405.1) at a redshift of z = 0.192. The light curve is compiled from photometry data of the All-sky Automated Survey for Supernovae (ASAS-SN)[17,18] V, ASAS-SN g, Zwicky Transient Facility (ZTF)[19] g, and ZTF r. The photometry data are calibrated to the ASAS-SN V band. After de-trending of the light curve, a sinusoid-like light curve emerges. The generalised Lomb-Scargle periodogram (GLS)[20] of the sinusoid-like light curve shows a strong and smooth periodic signal, corresponding to an observed period of $P_{\rm obs}$ = 726.8 $\pm$ 4.7 days. The total mass M and the orbital period of SMBBH in a circular orbit $P_{\rm orb}$ give an SMBBH separation of $d = 7.89 M_9^{1/3} (P_{\rm orb}/1.6{\rm yr})^{2/3}$ lt-days ($M_9 = M/10^9 M_{\odot}$). From M_9 = 2.0 (see Methods) and $P_{\rm orb}$ = 1.67 years, we obtain d = 10.2 lt-days = 0.009 parsec(pc) for PG 0923+201. As d $\lesssim$ 200 $r_{\rm g}$ ($r_{\rm g} = GM/c^2$ is the gravitational radius, G and c are the gravitational constant and the speed of light, respectively), the shrinking binary/circumbinary disk system eventually reaches a state in which the disk has decoupled from the rapidly shrinking binary[21,22]. For PG 0923+201, 200 $r_{\rm g}$ = 22.7 lt-days and then $d < 200\, r_{\rm g}$. Thus, the close SMBBH in PG 0923+201

is in the gravitational wave driven regime, where the SMBBH orbital shrink is driven by its gravitational wave emission. The rest-frame gravitational wave frequency f of a close SMBBH on circular orbits equals two times the orbital frequency, and $f \approx 2.7 \times 10^{-8}$ Hertz for PG 0923+201. Thus, PG 0923+201 is a candidate of Nano-Hertz gravitational wave source, which is expected to be detected by pulsar timing arrays.

The optical spectrum of PG 0923+201 in the SDSS shows the redward asymmetric profiles of the broad emission lines $\mathrm{H}\beta$ and $\mathrm{H}\alpha$ (Figures 2 and 3). A large number of active galactic nuclei (AGNs) show asymmetric profiles of broad emission lines, which are regarded as evidence of close SMBBHs[23]. The asymmetric profiles of broad emission lines of PG 0923+201 obviously differ from the double-peaked ones produced by the relativistic Doppler effects due to the orbital motion of individual BLRs of each SMBH in an SMBBH. Asymmetric line profiles are probably a far more common signature of SMBBHs than double-peaked broad line profiles that may be generated by SMBBHs with both distinct BLRs and only a narrow window of d[24]. This narrow window needs $d \gtrsim 0.14$ pc for PG 0923+201, which is not consistent with d = 0.009 pc we obtained. This implies why the $\mathrm{H}\beta$ and $\mathrm{H}\alpha$ broad emission lines only have the redward asymmetries rather than the double-peaked profiles for PG 0923+201.

Broad emission lines $\mathrm{H}\beta$ and $\mathrm{H}\alpha$ in PG 0923+201 have a radius of broad-line region (BLR) $R_{\mathrm{BLR}} \approx 115$ lt-days, and have full width at half maximum (FWHM) of FWHM $\approx$ 7700-8500 $\mathrm{km\,s^{-1}}$[25]. $R_{\mathrm{BLR}} \approx 115$ lt-days is much larger than d = 10.2 lt-days. However, $d \gtrsim 2R_{\mathrm{BLR}}$ is required in order to have a distinct BLR of each SMBH. Thus, the broad emission lines come from a much larger system enveloping the SMBBH in PG 0923+201, i.e, the SMBBH only has a circumbinary BLR and each SMBH should not have a distinct BLR. The low density central cavity would emerge because the circumbinary disk could be truncated by the central SMBBH's torques. The central cavity radius (the inner radius of the circumbinary disk) is about two times separation of SMBBH[9,26]. The cavity radius is about 20 lt-days for PG 0923+201, and the cavity is well within the circumbinary BLR.

The sinusoid fitting gives a variability amplitude of 0.301 $\pm$ 0.006 mJy. The average flux of the sinusoid-like variability is $\lesssim$ 2.6 mJy, because the long-term 3rd-order polynomial is $\sim$ 2.6

mJy at the beginning and this value is a sum of these two component contributions. We have ΔF_ν $\approx$ 0.3 mJy and $F_\nu \lesssim$ 2.6 mJy for the sinusoid-like variability. Thus, $\Delta F_\nu / F_\nu$ is $\gtrsim$ 0.12. $\Delta F_\nu / F_\nu$ = $\pm$(3 - α_ν) β cos φ sin i, where i and φ are the inclination and phase of the orbit, respectively[14]. The optical continuum spectrum of PG 0923+201 can be well described by a broken power-law with α_ν = 0.557 at the blue side[25]. The 0.3 mJy variability can be attributed to the relativistic Doppler boosting for a line-of-sight velocity amplitude of $v \times \sin(i) \gtrsim 0.05c$ = 15000 $\mathrm{km\,s^{-1}}$. This velocity amplitude is much higher than FWHM $\approx$ 7700–8500 km/s of the broad emission lines $\mathrm{H}\beta$ and $\mathrm{H}\alpha$, i.e., the FWHM is not produced by the orbital velocity of the secondary SMBH of the SMBBH in PG 0923+201 and there should not be individual BLR for the secondary SMBH.

The profiles around $\mathrm{H}\beta$ and $\mathrm{H}\gamma$ regions are very similar to each other in two observational periods: 1990.02.17 and 2005.12.01 (see Methods). This indicates the long-term stability of the hydrogen Balmer broad emission lines and the BLR in PG 0923+201. So, the ionizing continuum driving the broad emission lines is required to be long-lived. Simulations show that the two mini disks in an SMBBH can be long-lived[9]. A hotspot in accretion disk also may give rise to the periodic variability. If that is the case, the hot spot is at the distance of about 90 r_g from the central black hole. The hot spot is at the distance from 355 to 485 r_g for the broad-line radio galaxy Arp 102B with M = $10^{8.3}$ $M_\odot$[27]. Thus, it will be impossible for the existence of the hot spot at such a close distance for PG 0923+201. The jet precession could generate the variability with periods of larger than about several hundred years[3], which are much longer than the temporal baseline of about 9 years. Quasi-periodic variability in jetted AGNs can be caused due to orbiting blobs along helical trajectories[28]. The helical jet model predicts damping amplitude and increasing period of quasi-periodic variability for a few cycles in the light curve. However, this predicted variability does not emerge in the light curve of PG 0923+201. In addition, the jet in PG 0923+201 is excluded due to no detection of radio radiation[25]. A periodic variability of the optical luminosity will be expected from a warped disk. However, the precession timescale of a warp in accretion disk is too long to account for the observed optical variability of AGNs on timescales of a few years, e.g., Arp 102B[27]. Therefore, the SMBBH model is a robust interpretation of the periodic variability in PG 0923+201. The broad emission line profile variability may test the SMBBH hypothesis, e.g., double-peaked broad emission line variability of Arp 102B and 3C 390.3[29].

1. Graham, M. J., et al. A possible close supermassive black-hole binary in a quasar with optical periodicity. *Nature* **518**, 74-77 (2015).

2. D'Orazio, D. J., et al. A reduced orbital period for the supermassive black hole binary candidate in the quasar PG 1302-102?. *Mon. Not. R. Astron. Soc.* **452**, 2540-2545 (2015).

3. Lu, J. F., & Zhou, B. Y. Observational evidence of jet precession in galactic nuclei caused by accretion disks. *Astrophys. J.* **635**, L17-L20 (2005).

4. Begelman, M. C., Blandford, R. D. & Rees, M. J. Massive Black Hole Binaries in Active Galactic Nuclei. *Nature* **287**, 307-309 (1980).

5. EHT Collaboration, Akiyama, K., et al. First M87 Event Horizon Telescope Results. I. The Shadow of the Supermassive Black Hole. *Astrophys. J. Letters* **875**, L1 (2019).

6. LIGO Scientific Collaboration and Virgo Collaboration, Abbott, B. P., et al. Observation of Gravitational Waves from a Binary Black Hole Merger. *Phys. Rev. Lett* **116**, 061102 (2016).

7. Shi, J. M., Krolik, J. H., Lubow, S. H., & Hawley, J. F. Three-dimensional magnetohydrodynamic simulations of circumbinary accretion disks: disk structures and angular momentum transport. *Astrophys. J.* **749**, 118 (2012).

8. D'Orazio, D. J., Haiman, Z., & MacFadyen, A. Accretion into the central cavity of a circumbinary disc. *Mon. Not. R. Astron. Soc.* **436**, 2997-3020 (2013).

9. Farris, B. D., Duffell, P., MacFadyen, A. I., & Haiman, Z. Binary black hole accretion from a circumbinary disk: gas dynamics inside the central cavity. *Astrophys. J.* **783**, 134 (2014).

10. Shi, J. M., & Krolik, J. H. Three-dimensional MHD simulation of circumbinary accretion disks. II. Net accretion rate. *Astrophys. J.* **807**, 131 (2015).

11. Bowen, D. B., et al. Quasi-periodic Behavior of Mini-disks in Binary Black Holes Approaching Merger. *Astrophys. J. Letters* **853**, L17 (2018).

12. Moody, M. S. L., Shi, J. M., & Stone, J. M. Hydrodynamic Torques in Circumbinary Accretion Disks. *Astrophys. J.* **875**, 66 (2019).

13. Duffell, P. C., et al. Circumbinary Disks: Accretion and Torque as a Function of Mass Ratio and Disk Viscosity. *Astrophys. J.* **901**, 25 (2020).

14. D'Orazio, D. J., Haiman, Z., & Schiminovich, D. Relativistic boost as the cause of periodicity in a massive black-hole binary candidate. *Nature* **525**, 351-353 (2015).

15. Charisi, M., Haiman, Z., Schiminovich, D., & D'Orazio, D. J. Testing the relativistic Doppler boost hypothesis for supermassive black hole binary candidates. *Mon. Not. R. Astron. Soc.* **476**, 4617-4628 (2018).

16. Schneider, D. P., et al. The Sloan Digital Sky Survey Quasar Catalog. V. Seventh Data Release. *Astron. J.* **139**, 2360-2373 (2010).

17. Shappee, B. J., et al. The Man behind the Curtain: X-Rays Drive the UV through NIR Variability in the 2013 Active Galactic Nucleus Outburst in NGC 2617. *Astrophys. J.* **788**, 48 (2014).

18. Jayasinghe, T., et al. The ASAS-SN catalogue of variable stars III: variables in the southern TESS continuous viewing zone. *Mon. Not. R. Astron. Soc.* **485**, 961-971 (2019).

19. Masci, F. J., et al. The Zwicky Transient Facility: Data Processing, Products, and Archive. *Pub. Astron. Soc. Pac.* **131**, 018003 (2019).

20. Zechmeister, M., Kürster, M. The generalised Lomb-Scargle periodogram A new formalism for the floating-mean and Keplerian periodograms. *Astrophys. J.* **496**, 577-584 (2009).

21. Milosavljević, M., & Phinney, E. S. The Afterglow of Massive Black Hole Coalescence. *Astrophys. J.* **622**, L93-L96 (2015).

22. Haiman, Z., Kocsis, B., & Menou, K. The population of viscosity- and gravitational wave-driven supermassive black hole binaries among luminous active galactic nuclei. *Astrophys. J.* **700**, 1952-1969 (2009).

23. Du, P., et al. Monitoring AGNs with Hβ Asymmetry. I. First Results: Velocityresolved Reverberation Mapping. *Astrophys. J.* **869**, 142 (2018).

24. Shen, Y., & Loeb, A. Identifying supermassive black hole binaries with broad emission line diagnosis. *Astrophys. J.* **725**, 249-260 (2010).

25. Liu, H. Y., et al. A Comprehensive and Uniform Sample of Broad-line Active Galactic Nuclei from the SDSS DR7. *Astrophys. J. Supp.* **243**, 21 (2019).

26. Artymowicz, P., & Lubow, S. H. Dynamics of Binary-Disk Interaction. I. Resonances and Disk Gap Sizes. *Astrophys. J.* **421**, 651-667 (1994).

27. Newman, J. A., Eracleous, M., Filippenko, A. V., & Halpern, J. P. Measurement of an Active Galactic Nucleus Central Mass on Centiparsec Scales: Results of Long-Term Optical Monitoring of Arp 102B. *Astrophys. J.* **485**, 570-580 (1997).

28. Mohan, P., & Mangalam, A. Kinematics of and Emission from Helically Orbiting Blobs in A Relativistic Magnetized Jet. *Astrophys. J.* **805**, 91 (2015).

29. Doan, A., et al. An improved test of the binary black hole hypothesis for quasars with double-peaked broad Balmer lines. *Mon. Not. R. Astron. Soc.* **491**, 1104-1126 (2020).

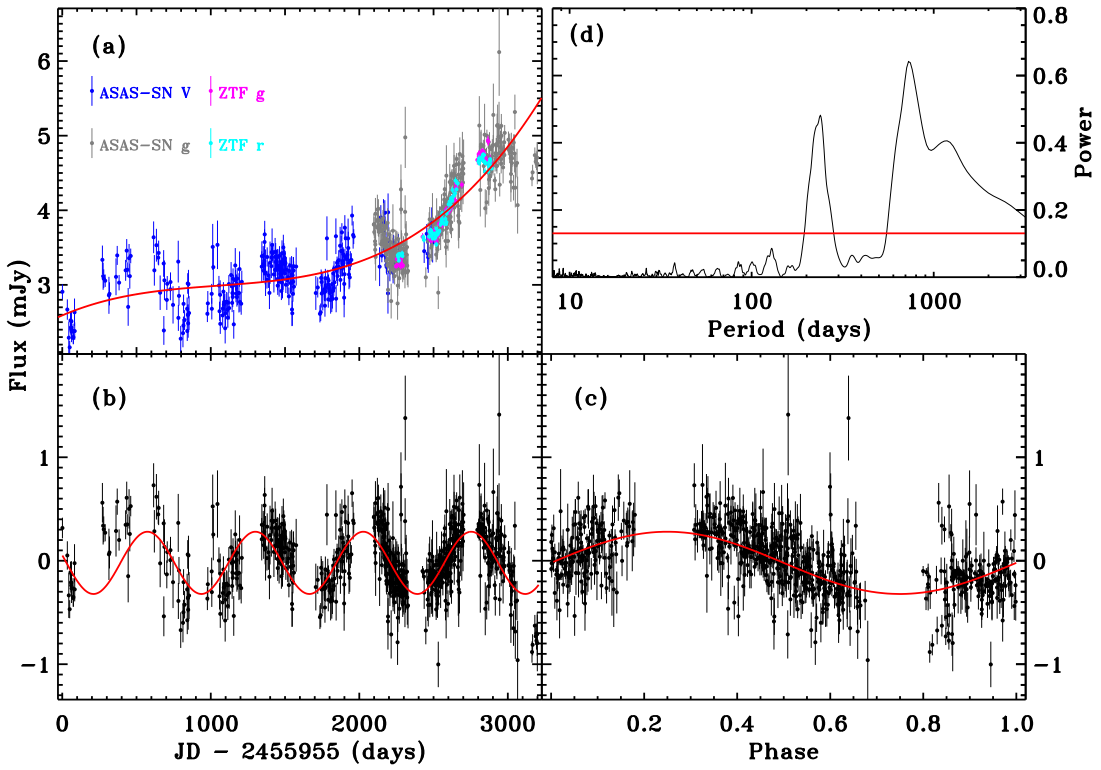

Figure 1: **Light curve and search for periodicity (see Methods for details).** Panel (a): the light curve of PG 0923+201, panel (b): the detrended light curve, panel (c): the bolded light curve, and panel (d): the GLS of the light curve in panel (b). Red curve in panel (a) denotes the third-order polynomials used to detrend the light curve. Red curves in panel (b) and (c) are the best-fit sinusoid. Red line in panel (d) denotes the GLS power at the confidence level of 99.999%.

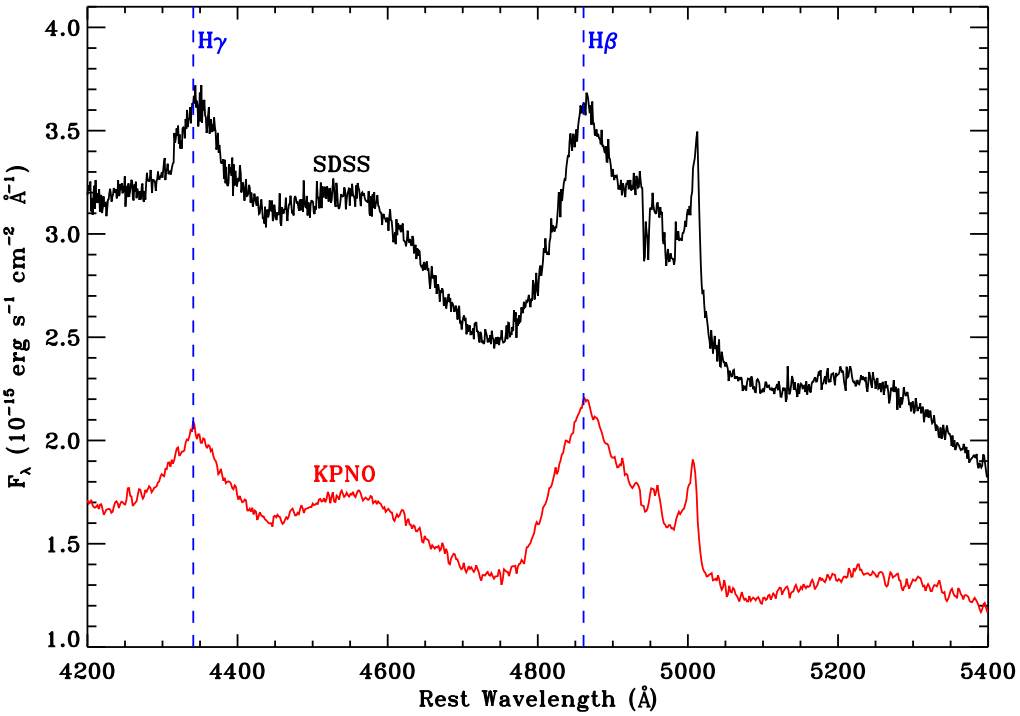

Figure 2: Red line: 1990.02.17 (KPNO), black line: 2005.12.01 (SDSS). There is no evidence of broad double-peaked profiles of the Balmer lines.

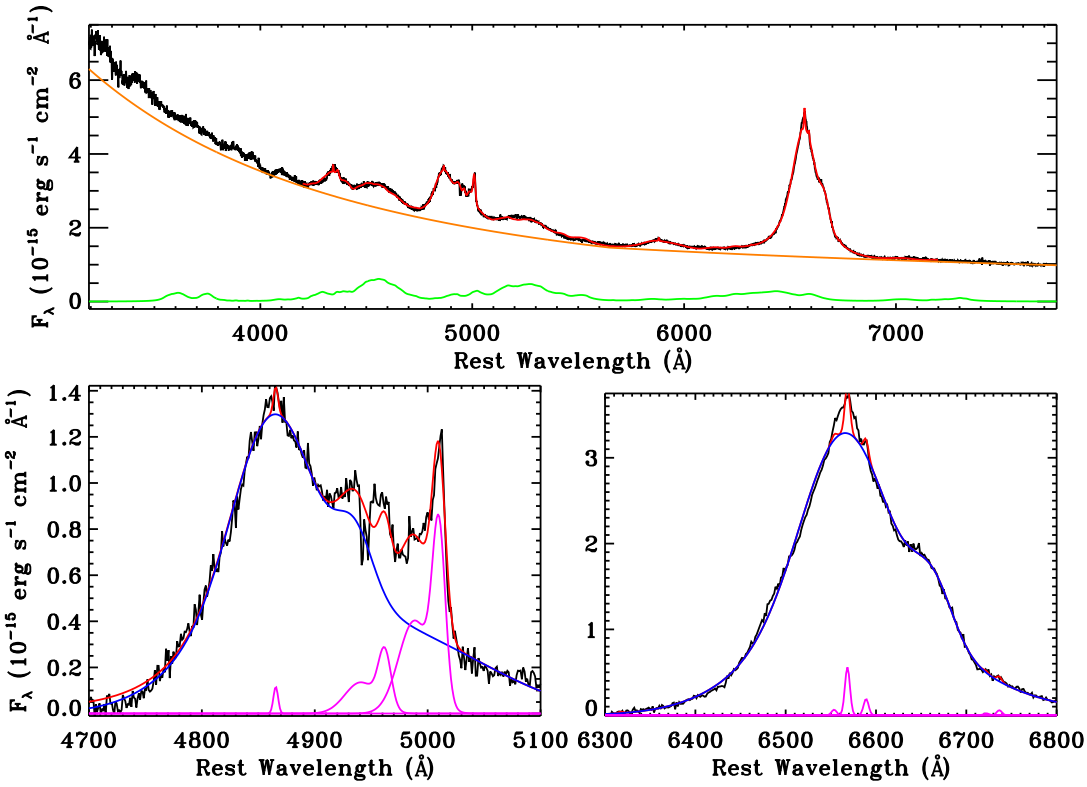

Figure 3: **The optical spectrum PG 0923+201: simultaneous fitting of the continuum and emission lines.** Top panel: the observed SDSS spectrum (black), the overall model (red), the AGN continuum (orange), and the Fe II multiplets (green). Bottom left panel: emission line profile fit to the Hβ+[O III] region. Bottom right panel: emission line profile fit to the Hα+[N II]+[S II] region. Bottom panels: the SDSS spectrum (black), the overall model (red), the fitted broad Hβ and Hα lines (blue), and the narrow lines (magenta).

Methods

Photometric and spectroscopic data. The All-sky Automated Survey for Supernovae (ASAS-SN) data are downloaded from http://www.astronomy.ohio-state.edu/asassn while the Zwicky Transient Facility (ZTF) data are downloaded from https://www.ztf.caltech.edu. We first remove some (9 ASAS-SN data points and 26 ZTF data points) outliers using a Gaussian filter. Then we convert all the magnitude into flux densities, and average the multiple observations within one night depending on their errors. Finally, the flux density in each individual band is scaled to ASAS-SN V band via $F_{sca} = C \times F_{obs}$. The scale factor C of every two bands can be calculated from the temporal overlap. We adopt a interval of 3 days for ASAS-SN V and ASAS-SN g and 1 day for other data sets. The intercalibrated light curve consists of 795 data points in a total temporal baseline of $\sim$ 9 years. To avoid introducing false period in our analysis, a low-order polynomial is used to subtract the long-term trend. We found that the detrended light curves from different polynomial degree (2-8 orders) are consistent with each other. A 3rd-order polynomial is adopted to detrend the intercalibrated light curve because of the minimum χ^2 in sinusoid fitting.

Figure 2 shows a comparison between two historical spectroscopic data taken on 1990 February 17 and 2005 December 01. The former spectrum is obtained from KPNO 2.1 m telescope[30], and the latter spectrum is from SDSS archival data. In order to extract valuable information from the spectrum, we employ the spectral fitting technique described in Ref.[25] to decompose the SDSS spectrum. The best-fit result is shown in Figure 3.

System parameters. For the black hole mass of this source, we adopted the results obtained in Ref.[25], who used the standard method of single epoch virial black hole estimation from the SDSS optical spectrum in Figure 3. The profiles of broad $\mathrm{H}\beta$ and $\mathrm{H}\alpha$ are common in AGNs, and obviously differ from the double-peaked broad emission lines produced by the Doppler effects due to the orbital motion of the individual BLR of each SMBH in the SMBBH. $\mathrm{H}\beta$ gives log($M_{\mathrm{H}\beta}/M_\odot$) = 9.31 and $\mathrm{H}\alpha$ gives log($M_{\mathrm{H}\alpha}/M_\odot$) = 9.27. $\mathrm{H}\alpha$ and $\mathrm{H}\beta$ jointly give log ($M/M_\odot$) = 9.29. These estimates are subject to an intrinsic scatter of 0.35 dex. Here, we adopt log ($M/M_\odot$) = 9.3 as the total mass of the SMBBH in PG 0923+201. The optical continuum luminosity at the rest-frame wavelength 5100Å is $L_{5100} \approx 10^{45}\ \mathrm{ergs\,s^{-1}}$, and the bolometric luminosity L_{bol} = 9.8 $\times$

10^{45} $\mathrm{ergs\,s^{-1}}$ ($L_{\rm bol}$ = $9.8L_{5100}$)[31]. The Eddington ratio of $L_{\rm bol}/L_{\rm Edd}$ is $\sim$ 0.04 (the Eddington luminosity $L_{\rm Edd}$ = $1.26 \times 10^{38} M/M_{\odot}$).

Statistical significance. For the generalised Lomb-Scargle (GLS) periodogram, there is a statistically significant peak of $P_{\rm obs}$ = 726.8 $\pm$ 4.7 days. The Baluev[33] estimate shows that the false alarm probability of this peak is $\ll 10^{-10}$– the 10^{-10} level is the power p = 0.1 and the observed peak is at p = 0.642. For the GLS periodogram, the bootstrap method[34] (implemented in astroML[32]) shows the false alarm probability of 10^{-5} corresponds to the power p = 0.13, i.e., p = 0.13 is at the confidence level of 99.999%. In order to remove artifacts due to seasonal gaps and cadences aliasing, $P_{\rm obs} < 400$ days is excluded from our periodicity detection. To minimize false periodicity from stochastic quasar variability[35], we remove any periodicity with $3P_{\rm obs} >$ the total time baseline, i.e., $P_{\rm obs} > 1100$ days. The reliability of the strongest peak is tested by the Monte Carlo simulation of 1000 realizations of the light curves generated with the model-independent random subset selection method, i.e., a randomly chosen subset of the detrended data points [36](Figure 4). About 63% ($\sim$ 1 - 1/e) of the data of the detrended light curve is randomly sampled in each realization.. Thus, the periodicity between 400 and 1100 days is not the false one resulting from the uneven sampling of the light curve.

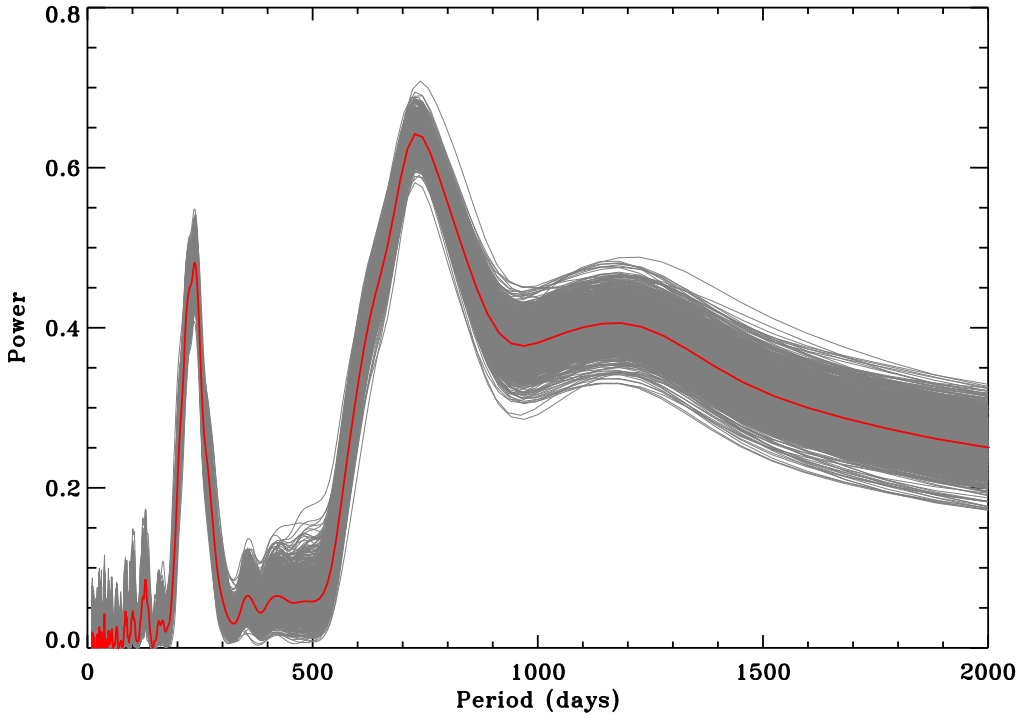

Figure 4: **The GLS of the light curve of PG 0923+201 (red line).** Gray lines are the GLS of the 1000 simulated light curves. Simulations show the reliability of the highest peak matching $400 < P_{\rm obs} < 1100$ days.

Acknowledgements This work is supported by the financial support of the National Natural Science Foundation of China (NSFC; grant No. 11991051). The authors thank H. Y. Liu for providing the fitting results of PG 0923+201. This work makes use of ASAS-SN and ZTF photometric data, and SDSS spectroscopic data. ZTF is based on observations obtained with the Samuel Oschin 48-inch Telescope at the Palomar Observatory as part of the Zwicky Transient Facility project. ZTF is supported by the National Science Foundation under Grant No. AST-1440341 and a collaboration including Caltech, IPAC, the Weizmann Institute for Science, the Oskar Klein Center at Stockholm University, the University of Maryland, the University of Washington, Deutsches Elektronen-Synchrotron and Humboldt University, Los Alamos National Laboratories, the TANGO Consortium of Taiwan, the University of Wisconsin at Milwaukee, and Lawrence Berkeley National Laboratories. Operations are conducted by COO, IPAC, and UW. Funding for the SDSS and SDSS-II has been provided by the Alfred P. Sloan Foundation, the Participating Institutions, the National Science Foundation, the U.S. Department of Energy, the National Aeronautics and Space Administration, the Japanese Monbukagakusho, the Max Planck Society, and the Higher Education Funding Council for England. The SDSS Web Site is http://www.sdss.org/. The SDSS is managed by the Astrophysical Research Consortium for the Participating Institutions. The Participating Institutions are the American Museum of Natural History, Astrophysical Institute Potsdam, University of Basel, University of Cambridge, Case Western Reserve University, University of Chicago, Drexel University, Fermilab, the Institute for Advanced Study, the Japan Participation Group, Johns Hopkins University, the Joint Institute for Nuclear Astrophysics, the Kavli Institute for Particle Astrophysics and Cosmology, the Korean Scientist Group, the Chinese Academy of Sciences (LAMOST), Los Alamos National Laboratory, the Max-Planck-Institute for Astronomy (MPIA), the Max-Planck-Institute for Astrophysics (MPA), New Mexico State University, Ohio State University, University of Pittsburgh, University of Portsmouth, Princeton University, the United States Naval Observatory, and the University of Washington.This research has made use of the NASA/IPAC Ex-

tragalactic Database (NED), which is funded by the National Aeronautics and Space Administration and operated by the California Institute of Technology.

Author Contributions B.J.M. conceived and supervised the project of searching for close SMBBHs. H.C.F. suggested the periodic variability in the source, performed the data analysis, and contributed to data points. H.T.L. interpreted the results and wrote the manuscript. H.T.L and H.C.F. performed calculation of the physical parameters of close SMBBH. B.J.M. and H.C.F. participated in the interpretation of the results. All the authors contributed to the interpretation of the results of the manuscript.

Author Information Reprints and permissions information is available at www.nature.com/reprints. Correspondence and requests for materials should be addressed to HCF(hcfeng@ynao.ac.cn), HTL(htliu@ynao.ac.cn), or JMB(baijinming@ynao.ac.cn).

Competing Interests The authors declare that they have no competing financial interests.

Data Availability The data that support the plots within this paper and other finding of this study are available from the corresponding authors upon reasonable request.

30. Boroson, T. A, & Green, R. F. The Emission-Line Properties of Low-Redshift Quasi-stellar Objects. *Astrophys. J. Supp.* **80**, 109-135 (1992).

31. McLure, R. J, & Dunlop, J. S. The cosmological evolution of quasar black hole masses. *Mon. Not. R. Astron. Soc.* **352**, 1390-1404 (2004).

32. Ivezić, Ž., Connolly, A. J., Vanderplas, J. T., & Gray, A. Statistics, Data Mining and Machine Learning in Astronomy. (Princeton Univ. Press, 2014).

33. Baluev, R. V. Assessing the statistical significance of periodogram peaks. *Mon. Not. R. Astron. Soc.* **385**, 1279-1285 (2008).

34. Süveges, M. Extreme-value modelling for the significance assessment of periodogram peaks. *Mon. Not. R. Astron. Soc.* **440**, 2099-2114 (2014).

35. Vaughan, S. et al. False periodicities in quasar time-domain surveys. *Mon. Not. R. Astron. Soc.* **461**, 3145-3152 (2016).

36. Peterson, B. S. et al. On Uncertainties in Cross-Correlation Lags and the Reality of Wavelength-dependent Continuum Lags in Active Galactic Nuclei. *Pub. Astron. Soc. Pac.* **110**, 660-670 (1998).

Figures

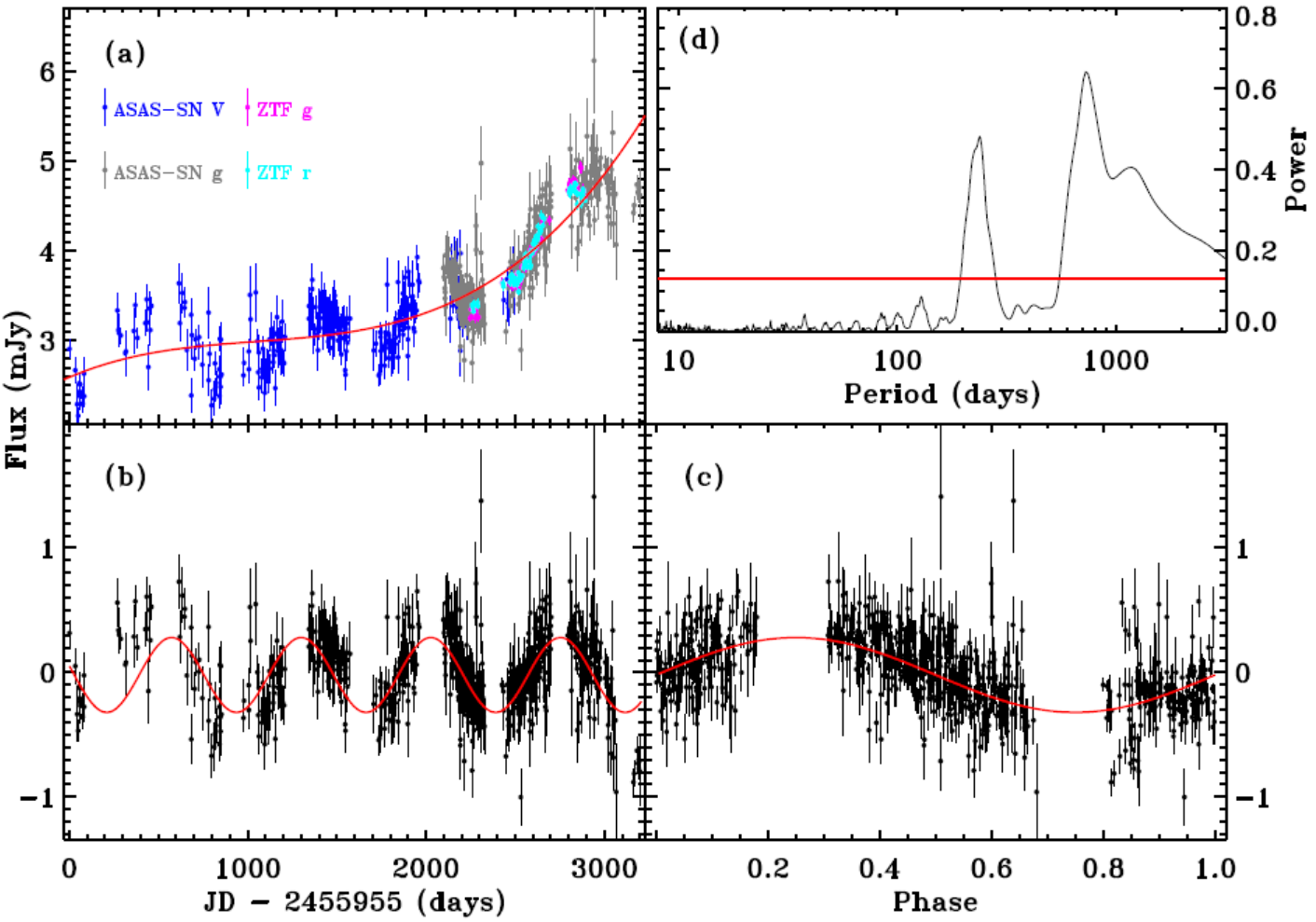

Figure 1

Light curve and search for periodicity (see Methods for details). Panel (a): the light curve of PG 0923+201, panel (b): the detrended light curve, panel (c): the bolded light curve, and panel (d): the GLS of the light curve in panel (b). Red curve in panel (a) denotes the third-order polynomials used to detrend the light curve. Red curves in panel (b) and (c) are the best-fit sinusoid. Red line in panel (d) denotes the GLS power at the confidence level of 99.999%.

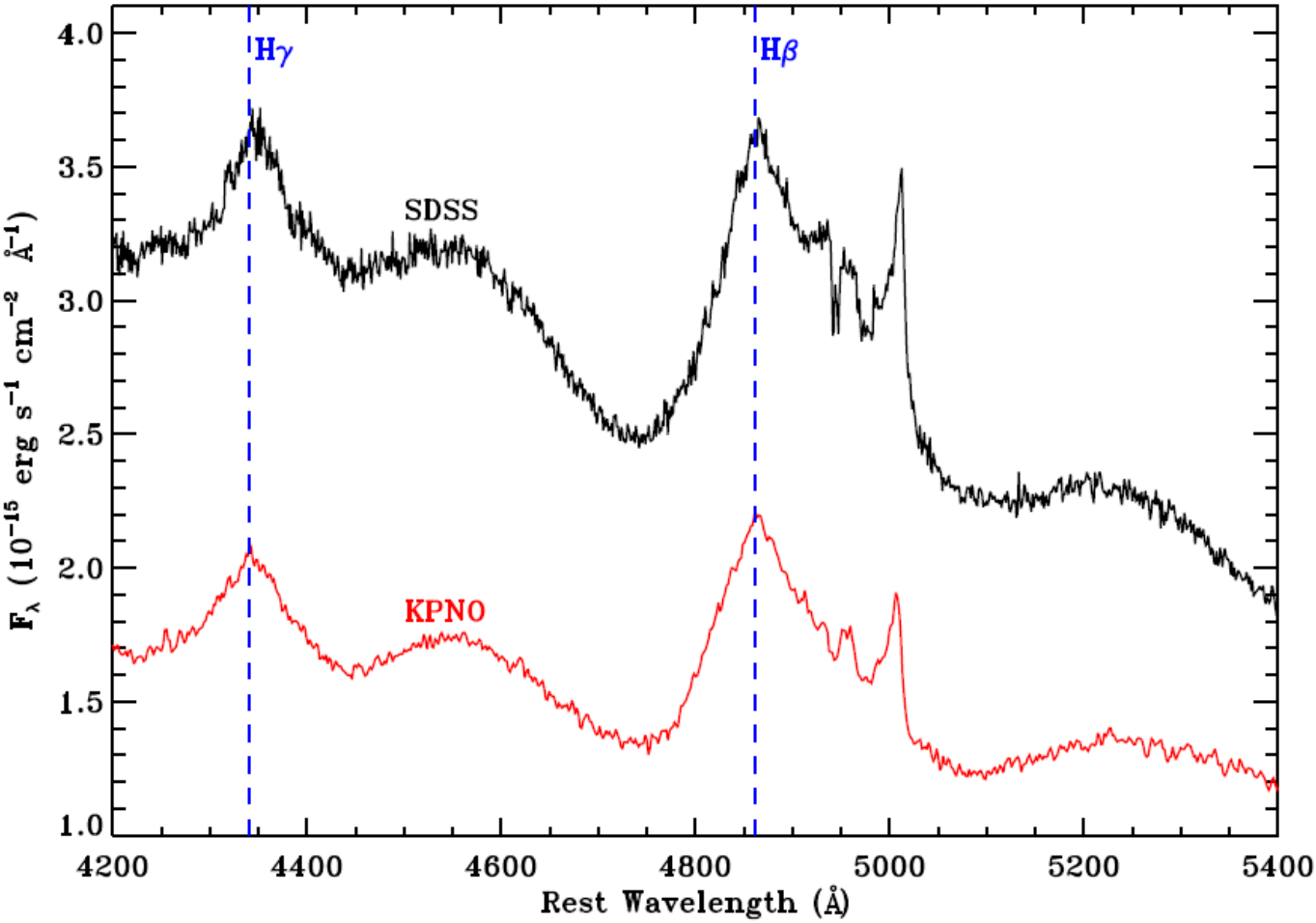

Figure 2

Red line: 1990.02.17 (KPNO), black line: 2005.12.01 (SDSS). There is no evidence of broad double-peaked profiles of the Balmer lines.

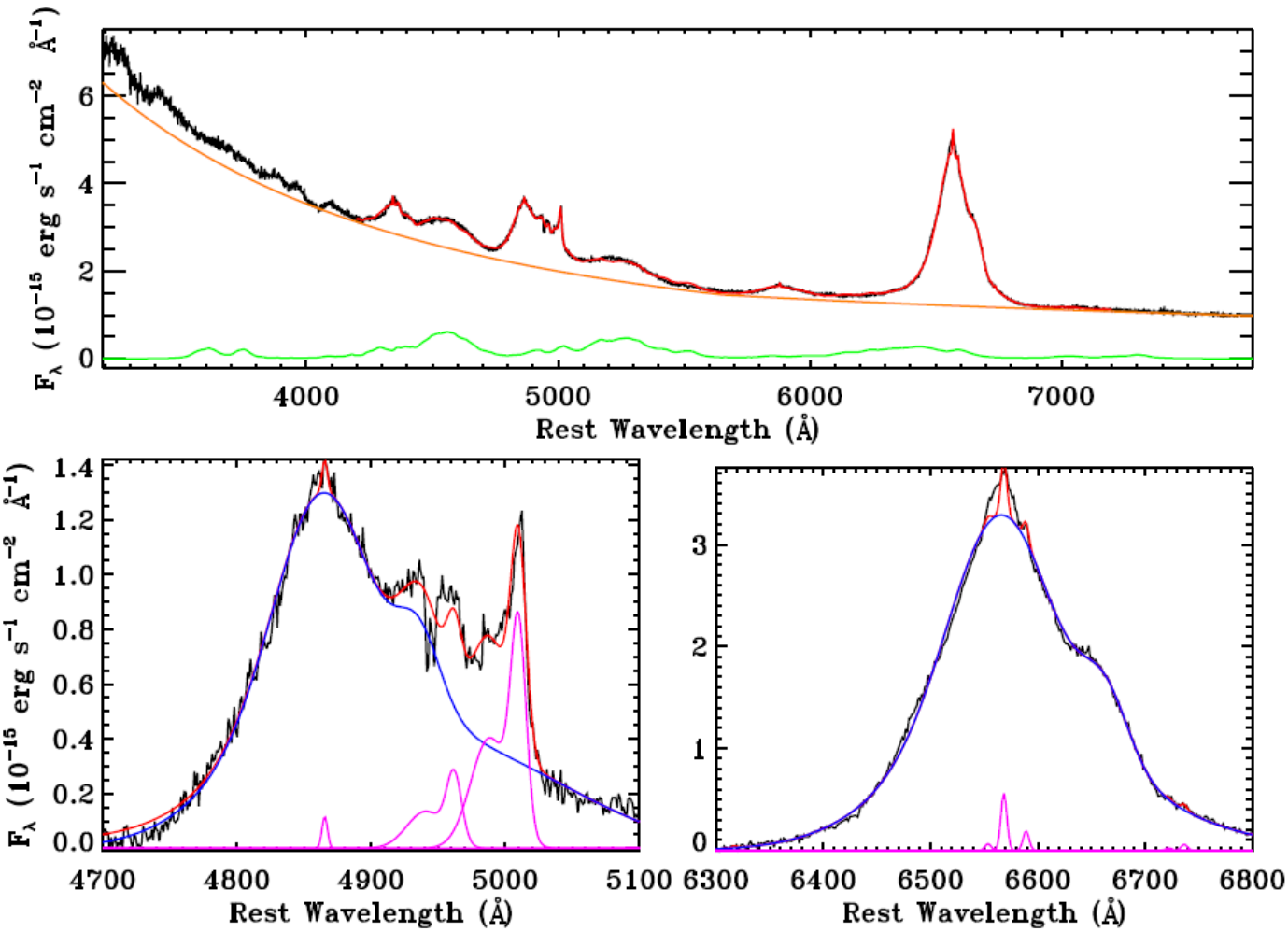

Figure 3

The optical spectrum PG 0923+201: simultaneous fitting of the continuum and emission lines. Top panel: the observed SDSS spectrum (black), the overall model (red), the AGN continuum (orange), and the Fe II multiplets (green). Bottom left panel: emission line profile fit to the Hβ+[O III] region. Bottom right panel: emission line profile fit to the Hα+[N II]+[S II] region. Bottom panels: the SDSS spectrum (black), the overall model (red), the fitted broad Hβ and Hα lines (blue), and the narrow lines (magenta).

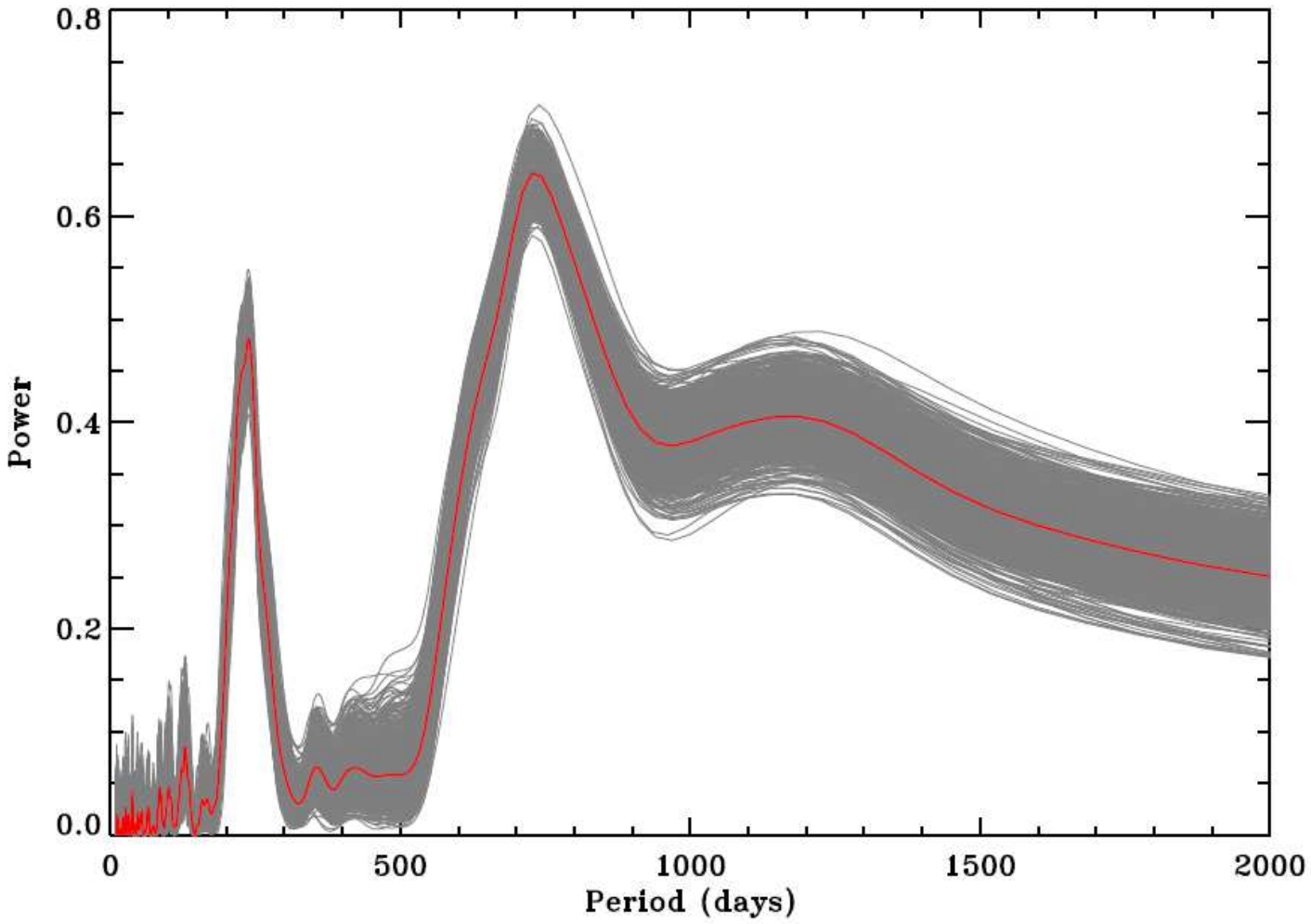

Figure 4

The GLS of the light curve of PG 0923+201 (red line). Gray lines are the GLS of the 1000 simulated light curves. Simulations show the reliability of the highest peak matching 400 < Pobs < 1100 days.